

Regional Heterogeneity in the Configuration of the Intracortical Canals of the Femoral Shaft

Egon Perilli¹ · Yohann Bala² · Roger Zebaze² · Karen J. Reynolds¹ · Ego Seeman³

Received: 8 December 2014 / Accepted: 12 May 2015 / Published online: 7 June 2015
© Springer Science+Business Media New York 2015

Abstract Three-dimensional (3D) characterization of cortical porosity, most of which is under 100 μm in diameter, is usually confined to measurements made in 3–4 mm diameter cylinders of bone. We used micro-computed tomography (micro-CT) scanning of entire transaxial cross sections of human proximal femoral shafts (30–35 mm diameter) to quantify regional variation in porosity within the same scan. Complete, up to 10-mm-thick, transaxial slices of femoral upper shafts from 8 female cadavers were studied ($n = 3$ aged 29–37 years, $n = 5$ aged 72–90 years). Scanning was performed using high-resolution micro-CT (8.65 $\mu\text{m}/\text{voxel}$). Micro-CT volumes (10 \times 10 \times 5 mm) were selected via software in the anterior, medial and lateral regions. Images were segmented with voids appearing as 3D-interconnected canals. The percent void-to-tissue volume (Vo.V/TV) and the corresponding void surface area/TV were 86–309 % higher in older than younger subjects in anterior ($p = 0.034$), medial ($p = 0.077$), and lateral aspects ($p = 0.034$). Although not significant, void separation was reciprocally lower by 19–39 %, and void diameter was 65 % larger in older than younger subjects; void number tended to be 24–25 % higher medially and laterally but not anteriorly. For all specimens combined, medially there was higher

Vo.V/TV and void surface area/TV than anteriorly (+48 %, $p = 0.018$; +33 %, $p = 0.018$) and laterally (+56 %, $p = 0.062$; +36 %, $p = 0.043$). There is regional heterogeneity in the 3D microarchitecture of the intracortical canals of the femoral shaft. The higher void volume in advanced age appears to be due to larger, rather than more, pores. However, creation of new canals from existing canals may contribute, depending on the location. High-resolution micro-computed tomography scanning of entire bone segments enables quantification of the 3D micro-anatomy of the intracortical void network at multiple locations.

Keywords Cortical bone · Micro-CT · Osteoporosis · Porosity · Voids

Introduction

Of all age-related appendicular bone loss, approximately 70 % is cortical and is the result of intracortical remodelling initiated upon Haversian canals in the cortex [1]. These canals are ‘seen’ as pores in cross-sectional images [2, 3]. The increase in cortical porosity compromises bone strength because cortical bone is placed peripherally, distant from the neutral axis of a long bone, conferring resistance to bending as a fourth power function of this distance [4]. Thus, quantification of cortical porosity, most of which is under 100 μm in diameter, plays an important role in identifying persons at risk for fracture and monitoring the effects of therapy [5–7].

Recent improvements in micro-computed tomography (micro-CT) scanners permit scanning entire bones as large as human vertebrae in vitro, at voxel sizes of $\sim 10 \mu\text{m}$ [8–10]. This method allows characterisation of the 3D

✉ Egon Perilli
egon.perilli@flinders.edu.au

¹ Medical Device Research Institute, School of Computer Science, Engineering and Mathematics, Flinders University, GPO Box 2100, Adelaide, SA 5001, Australia

² Department of Endocrinology, Austin Health, University of Melbourne, Melbourne, VIC, Australia

³ Departments of Endocrinology and Medicine, Austin Health, University of Melbourne, Melbourne, VIC, Australia

microarchitecture of cortical voids; the volume of the cortex occupied by voids, the diameter of the canals forming the voids, their surface area and separation [3, 11–13].

No study has been reported characterising the microarchitecture of cortical void structure in 3D using high-resolution micro-CT on entire human femoral cross sections. The aim of this study was to quantify cortical void morphology within entire human femoral diaphyseal cross sections at $8.65\ \mu\text{m}/\text{voxel}$ using a desktop 3D micro-CT system, in multiple locations.

Materials and Methods

Bone Specimens

Complete embedded transaxial femoral slices, up to 10-mm-thick in the longitudinal direction, prepared and used in a published study, were re-examined by micro-CT without further preparation or alteration [1]. Briefly, specimens of the right femur were removed from 8 female Caucasian cadavers. The women died from illnesses unrelated to bone disease (young: $n = 3$, age 29–37 years; old: $n = 5$, age 72–90 years). Specimens were stored at $-20\ ^\circ\text{C}$. For each cadaver, one complete transaxial slice up to 10-mm-thick (6 mm on average) was obtained 10 mm below the lesser trochanter. Specimens were dehydrated and embedded in methylmethacrylate [1]. The anatomical orientations (anterior, medial, lateral) were noted on the specimen, where the anterior aspect was defined as the region aligned with the centre of the cross section and the midpoint of the linea aspera [12].

Micro-CT Examination

The micro-CT examination was performed using a desktop micro-CT system (Skyscan 1076, Skyscan-Bruker NV, Kontich, Belgium). Scanning was performed with the bone specimen fixed on a carbon bed with the specimen axis in common with the rotation axis of the system. Scans were performed with a source voltage 100 kVp, current $80\ \mu\text{A}$, rotation step 0.2° , rotation over 180° , and a 1.0-mm-thick aluminium filter for beam hardening reduction. The isotropic pixel size was $8.65\ \mu\text{m}$, exposure time 4.1 s, 4 frames averaging and total scan duration 5 h 40 min for each specimen. The cross-section images were reconstructed using a filtered back projection algorithm (NRecon software, V 1.4.4, Skyscan-Bruker, Kontich, Belgium). For each specimen, a stack of up to 1200 contiguous cross sections was reconstructed with a slice thickness of 1 pixel ($8.65\ \mu\text{m}$) corresponding to a maximum reconstructed height up to 10.3 mm recreating the full height of the

specimen. The reconstructed axial cross-section images were of 4000×4000 pixels each, $8.65\ \mu\text{m}$ pixel size, corresponding to images of 34.6×34.6 mm. The volume scanned and reconstructed by micro-CT comprised the entire femoral cross section [8–10].

Selection of the Volume of Interest for Morphometric Analysis

From the stack of contiguous micro-CT cross-section images, volumes of interest (VOIs) were selected for morphometric analysis using a semi-automated method (software CTAnalyser V 1.13.5.1, Skyscan-Bruker, Kontich, Belgium). For each specimen, three (anterior, medial and lateral) VOIs were selected (Fig. 1). Each VOI was 10 mm long (circumferentially), 5 mm high (longitudinally, corresponding to 582 consecutive cross-section images) and up to 6 mm wide (radially) containing the

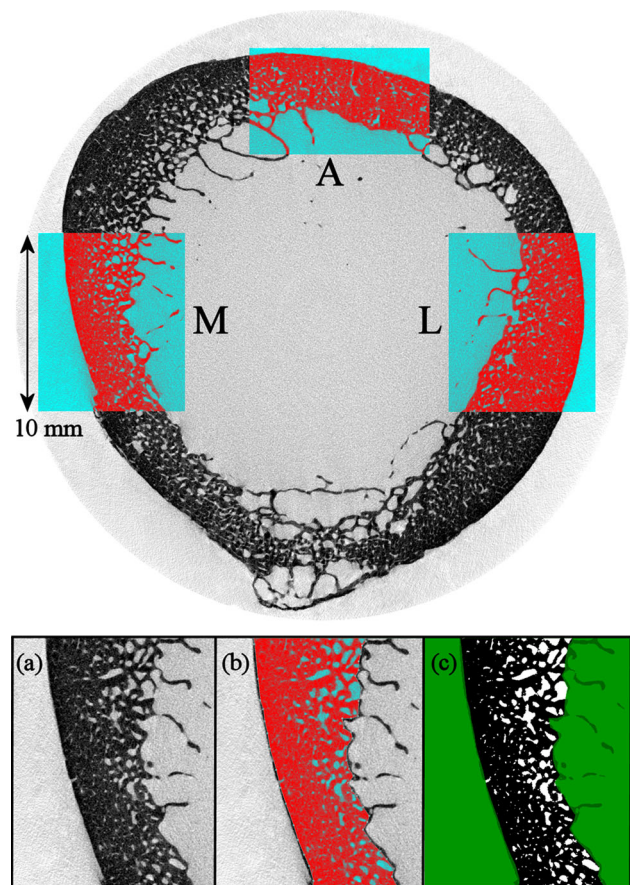


Fig. 1 Top micro-CT axial image of an entire femoral cross section ($8.65\ \mu\text{m}$ pixel size) showing anterior (A), medial (M) and lateral (L) regions of interest, all 10 mm long circumferentially. Bottom a medial location, selection of the region of interest for quantitative analysis (software CTAnalyser): *a* Grey level image, *b* contouring of the cortex, with the region of interest highlighted (voids in blue colour, bone in red colour), *c* thresholded image with voids within the region of interest in white colour and bone in black colour

entire cortex between the endosteal and periosteal envelopes. The cortex was contoured semiautomatically via software (Fig. 1), by the operator following the bordering pixels of the cortex every 30 cross sections (0.26 mm), and automatically interpolating over contiguous axial cross-section images (software CTAnalyser). 3D renderings of the micro-CT images of the medial region in the proximal shaft are shown in Fig. 2.

Morphometric Analysis

For each VOI, the tissue volume (TV, measured in mm^3) corresponded to the total volume analysed (bone plus void volumes, i.e. the VOI, Fig. 2) [14]. Within that volume, the voids were segmented as a solid and the mineralized bone as background using uniform thresholding [10]. The following morphometric parameters were calculated (software CTAnalyser) [12]: percentage void volume to tissue volume ($\text{Vo.V}/\text{TV}$, %), where void volume (Vo.V , mm^3) corresponds to the sum of the voxels segmented as voids; void surface area to tissue volume ($\text{Vo.S}/\text{TV}$, $1/\text{mm}$),

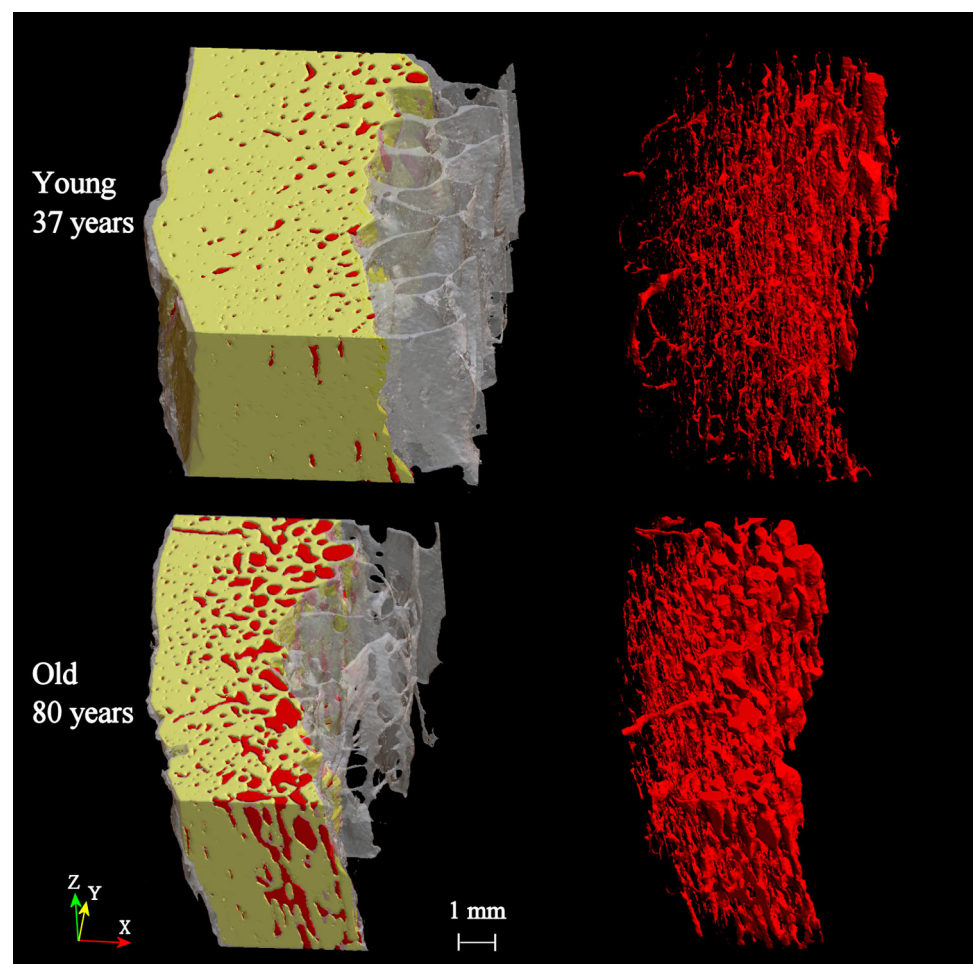
where the void surface area (Vo.S , mm^2) corresponds to the triangulated surface of the voids, calculated in 3D using the marching cube algorithm; void diameter (Vo.Diam , μm) and void separation (Vo.Sp , μm), which are the average diameter of the voids as a solid structure, and the average separation between the void structures, respectively, both calculated using direct 3D methods (sphere-fitting algorithm); and void number (Vo.N , $1/\text{mm}$), calculated as $\text{Vo.N} = 1/(\text{Vo.Sp} + \text{Vo.Diam})$, which corresponds to the reciprocal of the sum of void separation and void diameter, both calculated in 3D, as done by Cooper et al. [12, 15–18].

The cortical thickness was measured directly on the cross-section image and corresponded to the minimal distance between the periosteal and endosteal surface within the VOI (software CTAnalyser), with measurements taken every 26 images (225 μm) [3].

Statistical Analysis

For each anatomical region, comparisons of the morphometric parameters in the two age groups were performed

Fig. 2 3D rendering of micro-CT images (8.65 μm pixel size; rendered volumes 10 mm long circumferentially, 5 mm high longitudinally), medial location of the proximal shaft of the femur (as in Fig. 1), examples of bone from a young and old subject. *Left* Cortical volume of interest (VOI) for morphometric analysis highlighted in yellow colour, containing voids in red colour. *Right* voids segmented as solids in red colour, with bone removed (Color figure online)



using a non-parametric Mann–Whitney test (SAS software, SAS Inc, Cary, NC, USA). A within-subjects comparison was also done on all specimens, for testing for variations in the morphometric parameters among the three anatomical regions, using a non-parametric Friedman test followed by a Wilcoxon signed-rank test. The significance level for all comparisons was set at $p = 0.05$.

Results

Specimens from older subjects had a 261–309 % higher void volume/tissue volume and 163–165 % larger void surface area/tissue volume ratio relative to younger subjects in the anterior ($p = 0.034$) and lateral aspects ($p = 0.034$), with a trend in the medial region (+175 %, $p = 0.077$ for void volume/tissue volume, and +86 %, $p = 0.077$ for void surface area/tissue volume) (Table 1).

Void separation tended to be lower in older than younger subjects (28 % laterally, $p = 0.064$, and 39 % medially, $p = 0.077$). Void diameter tended to be 12–65 % higher in older than younger subjects [e.g. anteriorly,

average void diameter range 133–258 μm in older and 61–160 μm in younger subjects ($p = 0.16$)]. In the anterior region, the void number did not differ in older and younger subjects (+0.1 %, $p = 0.99$), whereas in older subjects it showed a trend to be higher laterally (+24 %, $p = 0.16$) and medially (+25 %, $p = 0.29$) (Table 1).

Figure 3 shows the distribution of void diameters grouped according to size in the three volumes of interest analysed, for the two age groups. Figures 4 and 5 show 3D renderings of the micro-CT images of the void network in the three volumes of interest, comparing old versus young.

When considering all the specimens combined, the void volume/tissue volume was 48 % higher in the medial than the anterior region ($p = 0.018$), with a similar trend in the medial compared to the lateral region (+56 %, $p = 0.062$, Fig. 6a). Consistent with this, there was a larger void surface area/tissue volume ratio medially than anteriorly (+33 %, $p = 0.018$) and laterally (+36 %, $p = 0.043$, Fig. 6b).

Cortical thickness was significantly lower in older than in younger subjects anteriorly (–26 %, $p = 0.034$), with a similar trend medially (–25 %, $p = 0.16$) and laterally (–22 %, $p = 0.16$) (Table 1).

Table 1 Intracortical morphometric parameters calculated in the anterior, medial and lateral VOI, for the two age groups

	Young (29–37 years)				Old (72–90 years)				Change (%)	<i>p</i>
	Avg	SD	Min	Max	Avg	SD	Min	Max		
Anterior										
Vo.V/TV (%)	3.11	2.48	2.40	5.49	11.23	3.31	7.29	14.90	261	0.034
Vo.S/TV (1/mm)	1.25	0.77	1.40	1.92	3.32	1.00	2.00	4.29	165	0.034
Vo.Diam (μm)	127	57	61	160	209	54	133	258	65	0.157
Vo.N (1/mm)	1.81	0.51	1.51	2.40	1.81	0.42	1.37	2.34	0.13	0.999
Vo.Sp (μm)	450	86	351	504	365	91	285	473	–19	0.157
Ct.Th (mm)	4.35	0.58	4.21	4.99	3.20	0.68	2.49	3.85	–26	0.034
Medial										
Vo.V/TV (%)	5.74	3.99	2.21	10.07	15.79	7.05	8.91	21.93	175	0.077
Vo.S/TV (1/mm)	2.17	1.47	0.65	3.60	4.04	0.84	3.09	5.13	86	0.077
Vo.Diam (μm)	171	37	143	214	191	50	136	254	12	0.724
Vo.N (1/mm)	1.64	0.56	1.00	2.00	2.05	0.32	1.66	2.43	25	0.289
Vo.Sp (μm)	503	248	342	788	307	44	262	347	–39	0.077
Ct.Th (mm)	4.66	0.41	4.40	5.13	3.49	0.99	2.63	4.58	–25	0.157
Lateral										
Vo.V/TV (%)	2.67	1.61	1.01	4.23	10.92	3.15	6.49	13.95	309	0.034
Vo.S/TV (1/mm)	1.24	0.69	0.60	1.96	3.25	0.56	2.62	3.82	163	0.034
Vo.Diam (μm)	153	63	101	223	192	63	113	265	25	0.480
Vo.N (1/mm)	1.56	0.25	1.39	1.74	1.93	0.28	1.56	2.24	24	0.165
Vo.Sp (μm)	469	41	440	498	336	31	302	377	–28	0.064
Ct.Th (mm)	4.86	0.39	4.54	5.30	3.79	1.05	2.91	4.88	–22	0.157

Average value (Avg); standard deviation (SD); minimum (min) and maximum (max) values; percentage change in average values in the old age group from the young age group (% change = $100 \times (\text{Avg}_{\text{old}} - \text{Avg}_{\text{young}})/\text{Avg}_{\text{young}}$); *p* value for non-parametric Mann–Whitney test in the comparison “old versus young”

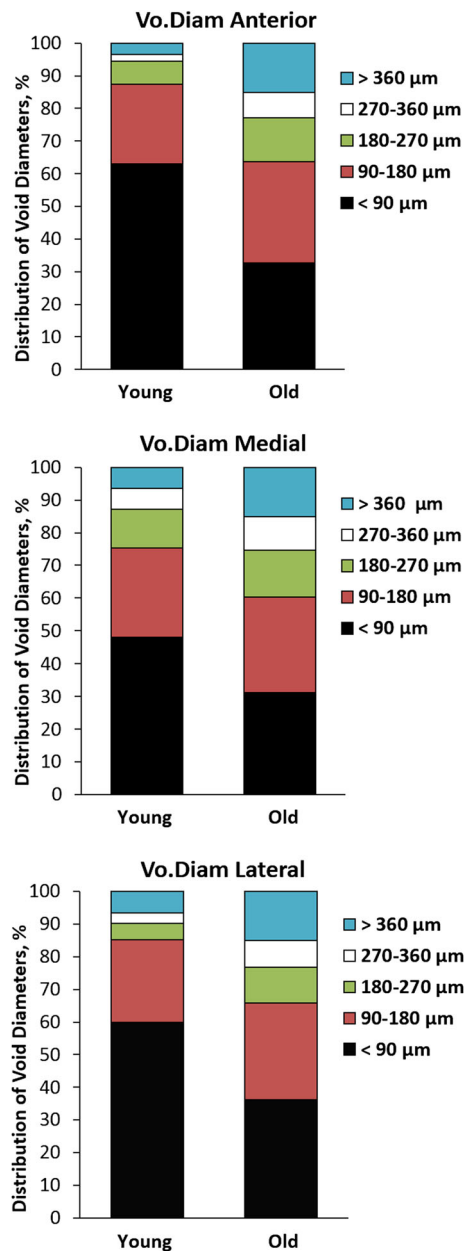


Fig. 3 Percentage distribution of the void diameters grouped according to size, in the anterior, medial and lateral VOI, for the two age groups

Discussion

This study provides a 3D analysis of the cortical void microstructure anteriorly, medially and laterally of entire human femoral diaphyseal cross sections. Specimens from older subjects had 175–309 % higher void volume and 86–165 % higher void surface area than younger subjects. In both the medial and lateral regions, void number and diameter of the voids showed a trend to increase. In the anterior region, the void diameter but not number tended to be higher in older than younger subjects. This last finding is

in agreement with previous reports using excised biopsy specimens at a single location (anterior) within the femur [12].

The trend for a higher intracortical canal diameter in advanced age suggests that it is the result of focal remodelling initiated upon existing canals formed during growth, with subsequent age-related focal enlargement of these canals, coalescence and formation of giant canals (Figs. 3–5) [5, 19, 20]. A trend for an increase in number of canals suggests that excavation of new canals may occur in parallel with existing canals, or perhaps with the appearance of new canals by remodelling initiated upon within osteocyte lacunar surfaces [21–23]. Further research is needed to examine the possible contribution of increased canal numbers to total void volume and if confirmed, how this may develop.

The statistically significant enlargement in void volume was accompanied by a corresponding significantly higher intracortical surface area and a trend in lower void separation (reflecting a smaller mineralized bone matrix volume), an appearance consistent with trabecularization of the cortex (Fig. 7). The enlargement of void at the price of mineralized bone matrix volume results in a larger void/matrix interface or surface area. When remodelling is signalled, either within the matrix perhaps by damaged osteocytes, within the marrow cavity or centrally, initiation of resorption takes place upon, and is facilitated by a larger, surface area. With a larger surface area, remodelling removes matrix further enlarging the void volume and creating more surface area upon which remodelling can be initiated. A vicious cycle of intracortical remodelling occurs that is responsible for most cortical bone loss which accounts for 70 % of all bone loss during ageing [1].

Comparing results obtained using 2D methods (as done on histological sections and microradiographs) versus 3D methods (through micro-CT) is problematic as pore diameter or surface is derived from the perimeter when 2D methods are used assuming that the pore is circular [24].

A study using 2D sections of the femoral midshaft reported that in specimens from younger persons the region showing highest porosity tended to be in the anterior lateral octant, whereas in the older persons in the anterior medial octant [25]. In another 2D study, the porosity was higher in the anterior octant compared to medial and lateral, in particular in the elderly population [2]. The present 3D study confirms that there are regional differences in the intracortical canal microstructure; the medial region had a significantly higher porosity than the anterior and lateral region, and a significantly higher void surface area to tissue volume than the anterior region with a similar trend in the lateral region. Hence, region-specific differences in void structure are likely and further investigation is needed to confirm this regional heterogeneity and explore the

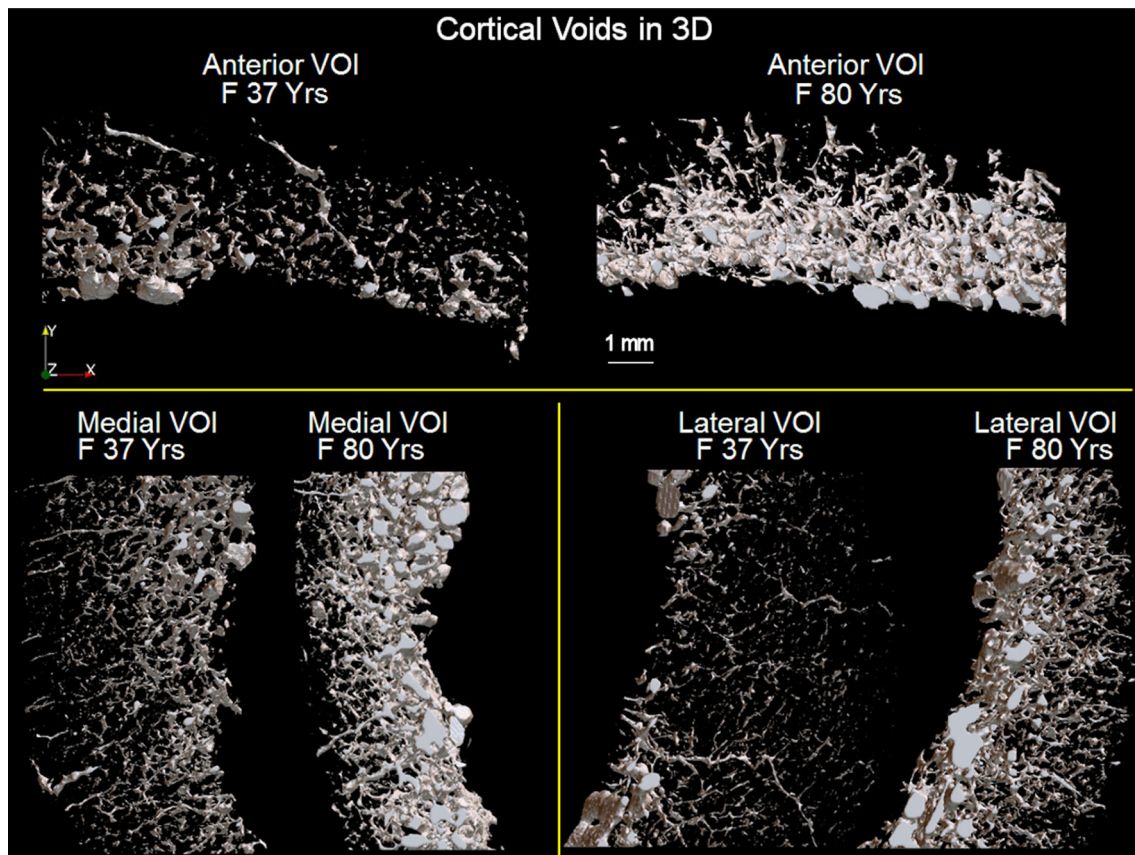


Fig. 4 3D rendering of the micro-CT images of the voids segmented as solids (here in *white colour*), which become visible as a 3D canal network, in the anterior, medial and lateral VOI. Examples of young (age 37 years) and old (age 80 years) subject. The VOIs are oriented

as shown in Fig. 1 (axis of the femur entering the page): the periosteal side is on top for the anterior VOI, on *left hand side* for the medial VOI, on *right hand side* for the lateral VOI

relevance to bone strength. While we found significant increases in porosity with age, from the data reported in Table 1, the regional distribution of porosity seems to not vary with age. The disparity compared to other studies could be due to differences in the location analysed along the femur (upper shaft in our manuscript, as opposed to midshaft in other papers), sex [25], or to small sample size ($n = 8$, compared to $n = 42$ [25], $n = 41$ [2]). We did not have information about loading history of the donors, which may influence regional porosity distribution and the effects of ageing [26–28].

The statistically significant thinner cortex in older compared to the younger subjects in the anterior region, with similar trend medially and laterally, is in agreement with previous microradiographic findings on femoral midshaft sections from female donors of age similar to this study [29]. Moreover, in both the age groups, the Ct.Th tended to be thinnest anteriorly compared to medially and laterally, in agreement with earlier reports [29].

It has been suggested that voxel sizes smaller than $10 \mu\text{m}$ are necessary to obtain consistent values of cortical void microarchitecture parameters calculated by micro-CT

[3, 11]. This condition was fulfilled using a voxel size of $8.65 \mu\text{m}$ to obtain micro-CT images of the entire femoral cross section [12].

The mean values of the 3D void parameters reported in this study are comparable with those reported using synchrotron micro-CT examination of excised cortical specimens from the upper shaft (cores from medial location), and those examining cylindrical cores from the femoral midshaft using a desktop micro-CT system (cores from anterior location 3–4 mm) [3, 12].

In the published literature, whereas the characterisation of the 3D bone microarchitecture of entire human bones at this high resolution has been done, the characterisation of the 3D microarchitecture of the cortical voids (void volume, void diameter, void surface, void separation) is still restricted to the analysis of small excised cortical bone biopsies, of few mm diameter (3–4 mm, recently $\sim 10 \text{ mm}$) [11–13, 30, 31]. This is labour intensive and particularly destructive if multiple coring is required and also obscures regional variation if measured in only one site (e.g. anteriorly) [12].

Within the limits of the gantry size of the specific micro-CT scanner used, the high-resolution micro-CT analysis

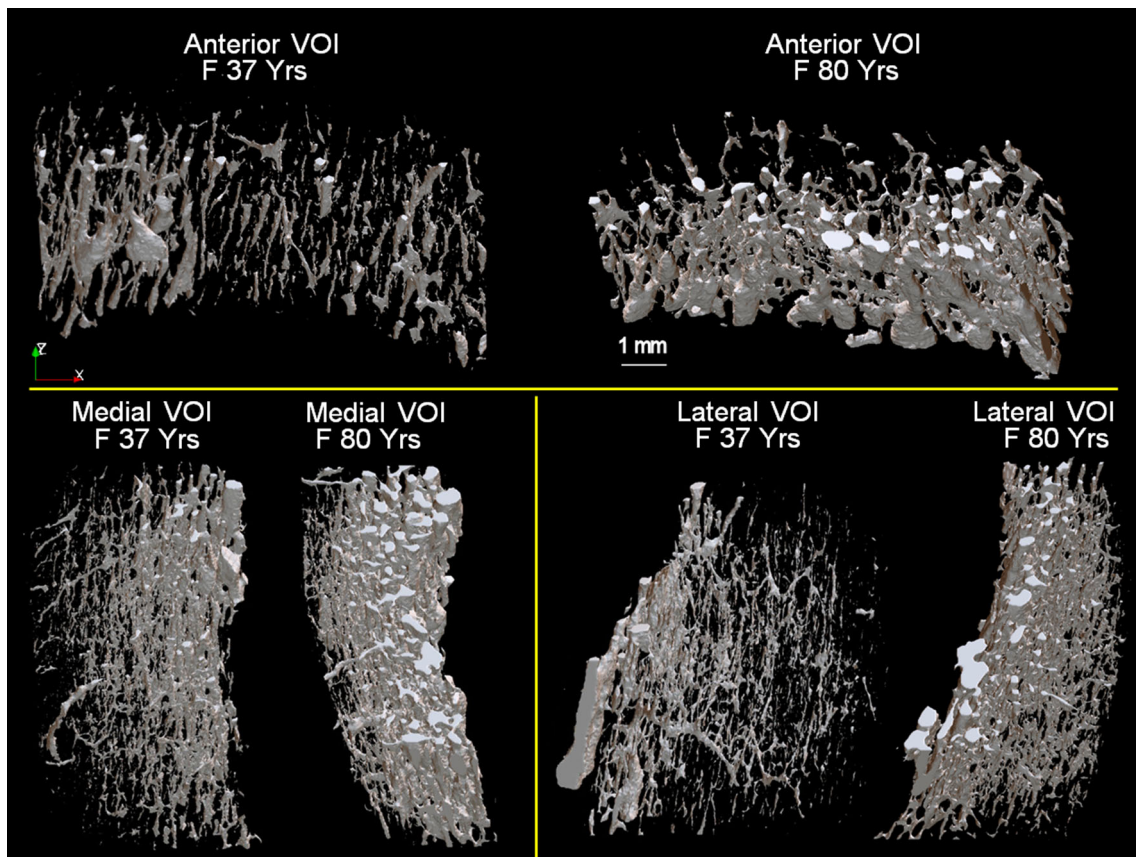
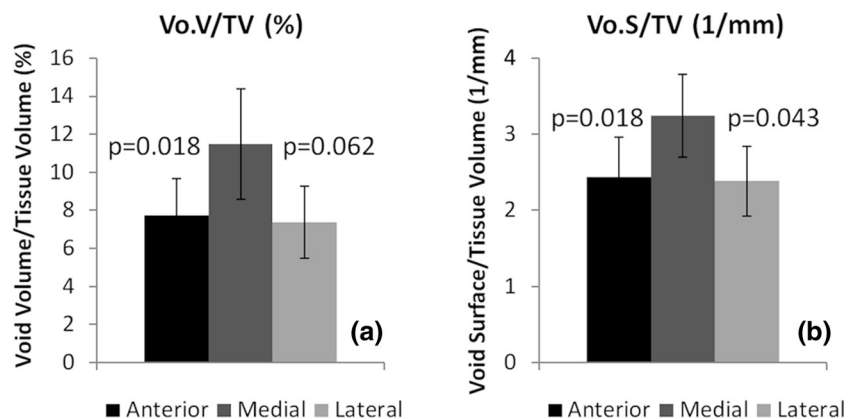


Fig. 5 3D rendering of the micro-CT images of the voids segmented as solids (in white colour, as in Fig. 4). The voids are slightly rotated in the 3D space compared to Fig. 4, for a visual appreciation of the 3D canal network in 3D

Fig. 6 3D micro-CT analysis, bar diagram of average value and standard error of the mean (error bars) of: **a** percentage void volume to tissue volume (indicated in %) and **b** void surface to tissue surface (indicated 1/mm), for the anterior, medial and lateral region. The indicated *p* value is for the non-parametric Wilcoxon signed-rank test



procedure used in this study on thick entire femoral shaft sections can be used to characterise the heterogeneity in void microstructure in larger bone segments up to entire bones, enabling also the investigation of the biomechanical role of these cortical voids, at the organ level [8, 9]. Micro-finite element analysis within segments of long bones could be performed, taking into account also the heterogeneity of the microstructure of the cortical pore networks [13].

A limitation of this study is the sample size (8 cadaveric specimens), which nonetheless allowed us to demonstrate the capability of high-resolution micro-CT, to characterise voids in 3D on entire cross sections of the human proximal femur in multiple and large volumes of interest. To account for the small sample size, we used non-parametric statistics (Mann–Whitney test, Friedman test and Wilcoxon signed-rank test) instead of parametric statistics, for comparison

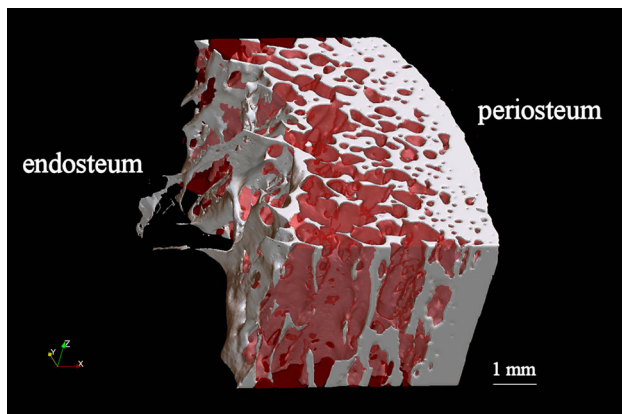


Fig. 7 3D rendering of a micro-CT volume in lateral location of the femoral cross section, voids in red colour, bone in white colour. Examples of old (age 86 years) subject, where large voids have coalesced, leading to trabecularization of the cortex (Color figure online)

between the two age groups or among regions. To test the effects of age on cortical pore microarchitecture in an adequately powered study, with $\alpha = 0.05$ and power = 80 %, for a sought effect size of 1 standard deviation, $n = 17$ specimens per group would have been needed [32]. Hence, non-statistically significant differences between young and old should be interpreted with caution. Another limitation was the limited amount of information available regarding the donors. Further research is needed to study the regional heterogeneity of cortical voids microarchitecture in 3D.

Within the confines of the limited sample size, we confirm that there is regional heterogeneity in the 3D microarchitecture of the intracortical canals of the upper femoral shaft. In the aged group, there is a significantly higher pore volume to tissue volume, with corresponding higher surface area to tissue volume. The higher void volume is likely to be the result of enlargement of existing canals rather than number, in agreement with previous reports, and reflects unbalanced and rapid remodelling upon surfaces of Haversian and Volkmann canals formed during growth [2, 24, 25, 33–35]. The age-related changes in void microstructure appear to depend on anatomical location. High-resolution micro-CT imaging of entire femoral bone segments provides a quantitative means of studying the 3D microanatomy of the intracortical canal network in multiple anatomical locations.

Acknowledgments Funding for this study was provided by Osteoporosis Australia/Australia New Zealand Bone and Mineral Society, Amgen-GSK Grants Program 2012.

Conflict of Interest Egon Perilli, Yohann Bala, Roger Zebaze, Karen J Reynolds, and Ego Seeman declare that they have no conflict of interest.

Human and Animal Rights and Informed Consent All procedures performed in studies involving human participants were in accordance with the ethical standards of the institutional and/or national research committee and with the 1964 Helsinki declaration and its later amendments or comparable ethical standards.

References

- Zebaze RM, Ghasem-Zadeh A, Bohte A, Iuliano-Burns S, Mirams M, Price RI, Mackie EJ, Seeman E (2010) Intracortical remodelling and porosity in the distal radius and post-mortem femurs of women: a cross-sectional study. *Lancet* 375:1729–1736
- Thomas CD, Feik SA, Clement JG (2006) Increase in pore area, and not pore density, is the main determinant in the development of porosity in human cortical bone. *J Anat* 209:219–230
- Chappard C, Bensalah S, Olivier C, Gouttenoire PJ, Marchadier A, Benhamou C, Peyrin F (2013) 3D characterization of pores in the cortical bone of human femur in the elderly at different locations as determined by synchrotron micro-computed tomography images. *Osteoporos Int* 24:1023–1033
- Whiting WC, Zernicke RF (2008) Biomechanics of musculoskeletal injury. 2nd ed, Publisher: Human Kinetics, Champaign: chapter 3 basic biomechanics, material mechanics 80–92
- Bell KL, Loveridge N, Power J, Garrahan N, Meggitt BF, Reeve J (1999) Regional differences in cortical porosity in the fractured femoral neck. *Bone* 24:57–64
- McCalden RW, McGeough JA, Barker MB, Court-Brown CM (1993) Age-related changes in the tensile properties of cortical bone. The relative importance of changes in porosity, mineralization, and microstructure. *J Bone Joint Surg Am* 75:1193–1205
- Bala Y, Chapurlat R, Cheung AM, Felsenberg D, LaRoche M, Morris E, Reeve J, Thomas T, Zanchetta J, Bock O, Ghasem-Zadeh A, Djoumessi RM, Seeman E, Rizzoli R (2014) Risedronate slows or partly reverses cortical and trabecular microarchitectural deterioration in postmenopausal women. *J Bone Miner Res* 29:380–388
- Perilli E, Parkinson IH, Reynolds KJ (2012) Micro-CT examination of human bone: from biopsies towards the entire organ. *Ann Ist Super Sanita* 48:75–82
- Briggs AM, Perilli E, Parkinson IH, Wrigley TV, Fazzalari NL, Kantor S, Wark JD (2010) Novel assessment of subregional bone mineral density using DXA and pQCT and subregional microarchitecture using micro-CT in whole human vertebrae: applications, methods, and correspondence between technologies. *J Clin Densitom* 13:161–174
- Perilli E, Briggs AM, Kantor S, Codrington J, Wark JD, Parkinson IH, Fazzalari NL (2012) Failure strength of human vertebrae: prediction using bone mineral density measured by DXA and bone volume by micro-CT. *Bone* 50:1416–1425
- Cooper DM, Matyas JR, Katzenberg MA, Hallgrímsson B (2004) Comparison of microcomputed tomographic and microradiographic measurements of cortical bone porosity. *Calcif Tissue Int* 74:437–447
- Cooper DM, Thomas CD, Clement JG, Turinsky AL, Sensen CW, Hallgrímsson B (2007) Age-dependent change in the 3D structure of cortical porosity at the human femoral midshaft. *Bone* 40:957–965
- Donaldson FE, Pankaj P, Cooper DM, Thomas CD, Clement JG, Simpson AH (2011) Relating age and micro-architecture with apparent-level elastic constants: a micro-finite element study of female cortical bone from the anterior femoral midshaft. *Proc Inst Mech Eng H* 225:585–596
- Dempster DW, Compston JE, Drezner MK, Glorieux FH, Kanis JA, Malluche H, Meunier PJ, Ott SM, Recker RR, Parfitt AM

- (2013) Standardized nomenclature, symbols, and units for bone histomorphometry: a 2012 update of the report of the ASBMR Histomorphometry Nomenclature Committee. *J Bone Miner Res* 28:2–17
15. Ulrich D, van Rietbergen B, Laib A, Rügsegger P (1999) The ability of three-dimensional structural indices to reflect mechanical aspects of trabecular bone. *Bone* 25:55–60
 16. Hildebrand T, Rügsegger P (1997) A new method for the model-independent assessment of thickness in three-dimensional images. *J Microsc* 185:67–75
 17. Perilli E, Baruffaldi F, Bisi MC, Cristofolini L, Cappello A (2006) A physical phantom for the calibration of three-dimensional X-ray microtomography examination. *J Microsc* 222:124–134
 18. Lorensen WE, Cline HE (1987) Marching cubes: a high resolution 3D surface construction algorithm. *Comput Graph* 21:163–169
 19. Jordan GR, Loveridge N, Bell KL, Power J, Rushton N, Reeve J (2000) Spatial clustering of remodeling osteons in the femoral neck cortex: a cause of weakness in hip fracture? *Bone* 26:305–313
 20. Cadet ER, Gafni RI, McCarthy EF, McCray DR, Bacher JD, Barnes KM, Baron J (2003) Mechanisms responsible for longitudinal growth of the cortex: coalescence of trabecular bone into cortical bone. *J Bone Joint Surg Am* 85-A:1739–1748
 21. Atkins GJ, Findlay DM (2012) Osteocyte regulation of bone mineral: a little give and take. *Osteoporos Int* 23:2067–2079
 22. Teti A, Zallone A (2009) Do osteocytes contribute to bone mineral homeostasis? Osteocytic osteolysis revisited. *Bone* 44:11–16
 23. Qing H, Ardeshirpour L, Pajevic PD, Dusevich V, Jahn K, Kato S, Wysolmerski J, Bonewald LF (2012) Demonstration of osteocytic perilacunar/canalicular remodeling in mice during lactation. *J Bone Miner Res* 27:1018–1029
 24. Stein MS, Feik SA, Thomas CD, Clement JG, Wark JD (1999) An automated analysis of intracortical porosity in human femoral bone across age. *J Bone Miner Res* 14:624–632
 25. Martin RB, Pickett JC, Zinaich S (1980) Studies of skeletal remodeling in aging men. *Clin Orthop Relat Res* 149:268–282
 26. Biewener AA (1991) Musculoskeletal design in relation to body size. *J Biomech* 24(Suppl 1):19–29
 27. Lanyon LE (1992) The success and failure of the adaptive response to functional load-bearing in averting bone fracture. *Bone* 13(Suppl 2):S17–S21
 28. Thomas CD, Feik SA, Clement JG (2005) Regional variation of intracortical porosity in the midshaft of the human femur: age and sex differences. *J Anat* 206:115–125
 29. Feik SA, Thomas CD, Bruns R, Clement JG (2000) Regional variations in cortical modeling in the femoral mid-shaft: sex and age differences. *Am J Phys Anthropol* 112:191–205
 30. Ostertag A, Peyrin F, Fernandez S, Laredo JD, de Vernejoul MC, Chappard C (2014) Cortical measurements of the tibia from high resolution peripheral quantitative computed tomography images: a comparison with synchrotron radiation micro-computed tomography. *Bone* 63:7–14
 31. Bousson V, Peyrin F, Bergot C, Hausard M, Sautet A, Laredo JD (2004) Cortical bone in the human femoral neck: three-dimensional appearance and porosity using synchrotron radiation. *J Bone Miner Res* 19:794–801
 32. Lieber RL (1990) Statistical significance and statistical power in hypothesis testing. *J Orthop Res* 8:304–309
 33. Bousson V, Meunier A, Bergot C, Vicaud E, Rocha MA, Morais MH, Laval-Jeantet AM, Laredo JD (2001) Distribution of intracortical porosity in human midfemoral cortex by age and gender. *J Bone Miner Res* 16:1308–1317
 34. Jowsey J (1960) Age changes in human bone. *Clin Orthop Relat Res* 38:210–217
 35. Atkinson PJ (1965) Changes in resorption spaces in femoral cortical bone with age. *J Pathol Bacteriol* 89:173–178